# Partial structure factors of liquid al80 (mnx(fecr) 1-x)20 alloys

M. Maret, A. Pasturel, C. Senillou, J.M. Dubois, P. Chieux

*J. Phys. France* **50** (1989) 295-310 1er FÉVRIER **1989,** PAGE 295

Classification
*Physics Abstracts*
61.12 — 61.25

# Partial structure factors of liquid $Al_{80}(Mn_x(FeCr)_{1-x})_{20}$ alloys

M. Maret (1), A. Pasturel (1), C. Senillou (1), J. M. Dubois (2) and P. Chieux (3)

(1) Laboratoire de Thermodynamique et Physico-Chimie Métallurgiques, CNRS UA 29, ENSEEG, BP 75, 38402 Saint Martin d'Hères Cedex, France
(2) Laboratoire de Science et Génie des Matériaux Métalliques, ENSMIN, Parc de Saurupt, 54042 Nancy Cedex, France
(3) Institut Laue Langevin, BP 156 X, 38042 Grenoble Cedex, France

(*Reçu le 5 septembre 1988, accepté le 11 octobre 1988*)

**Résumé.** — La structure des alliages liquides $Al_{80}(Mn_x(FeCr)_{1-x})_{20}$ a été étudiée par diffraction neutronique en utilisant la substitution entre les atomes de Mn et le mélange $\sigma$-FeCr. Nous avons vérifié que cette substitution est isomorphe en réalisant quatre expériences sur des mélanges différents tels que $x = 1$, 0,639, 0,304 et 0. Les facteurs de structure partiels de Bhatia-Thornton et de Faber-Ziman ont été déterminés et, en particulier, certaines caractéristiques dans la fonction $S_{NN}$ et dans la fonction de distribution des paires d'atomes de métal de transition mettent en évidence l'existence d'un ordre topologique bien défini. Toutefois, une simple comparaison des distances interatomiques et des nombres de coordination partiels dans les phases liquide, quasi-cristalline et cristalline est insuffisante pour définir le type d'ordre local. Les effets d'ordre chimique dans ces alliages liquides sont peu marqués avec un paramètre d'ordre local chimique égal à $-0{,}05$.

**Abstract.** — The structure of the liquid $Al_{80}(Mn_x(FeCr)_{1-x})_{20}$ alloys has been studied using neutron diffraction and the substitution between Mn atoms and the $\sigma$-FeCr mixture. We have checked that this substitution is isomorphous by performing four measurements on different mixtures with $x = 1$, 0.639, 0.304 and 0. The Bhatia-Thornton as well as the Faber-Ziman partial structure factors have been determined and in particular, certain features in the $S_{NN}$ function and in the distribution of transition metal atom pairs point out to the existence of a well-defined topological ordering. But a simple comparison between the interatomic distances and partial coordination numbers in the liquid, quasicrystalline and crystalline phases is still insufficient to characterize clearly the type of local order. The chemical ordering effects in these liquid alloys are relatively moderate with a chemical short-range order parameter of $-0.05$.

## 1. Introduction.

The knowledge of the atomic structure of disordered binary systems described by three partial structure factors (PSF) is necessary for the calculation of their electronic density of states and more generally for the understanding of their electronic properties.

At the moment, we focus our attention on the structure of liquid transition metal-aluminium alloys. The discovery of icosahedral phases of AlMn [1] and the large scattering

contrast brought by the isomorphous substitution between Mn atoms and the $\sigma$-FeCr mixture in neutron diffraction (used previously in quasicrystalline phases [2]) have encouraged us to study the structure of the pseudo-binary liquid $Al_{80}(Mn_x(FeCr)_{1-x})_{20}$ alloys. Of course, one of the first points will be to confirm the isomorphous behaviour between Mn atoms and the $\sigma$-FeCr mixture in the liquid phase by performing four neutron diffraction measurements with different Mn to $\sigma$-FeCr atomic ratios ; the fourth measurement allows us to check the consistency of the 3 PSFs extracted from the three others.

It will be interesting to compare the local order of the liquid phase with those previously determined by neutron diffraction in the icosahedral $Al_{74}Si_5Mn_{21}$ and decagonal $Al_{80}Mn_{20}$ phases [3, 4] and also in their crystalline hexagonal $\beta$-$Al_9SiMn_3$ [3] modification. Actually, if an icosahedral bond orientational order has been shown in computer experiments on supercooled liquids [5], such an order has not yet been observed above the liquidus.

There exists several definitions of partial structure factors for a binary liquid. Here, we will be interested in the determination of the Bhatia Thornton $S_{N,C}(Q)$'s [6] and the Faber Ziman $I_{ij}(Q)$'s [7]. There are related to the coherent scattering cross-section per atom, $d\sigma_{coh}/d\Omega(Q)$, as follows :

$$S(Q) = \frac{d\sigma_{coh}}{d\Omega}(Q)/\langle b^2\rangle = \sum_{N,C} W_{NC}\, S_{N,C}(Q)$$

more explicitly :

$$S(Q) = \frac{\langle b\rangle^2}{\langle b^2\rangle} S_{NN}(Q) + \frac{2\,\Delta b\,\langle b\rangle}{\langle b^2\rangle} S_{NC}(Q) + \frac{c_T\, c_{Al}(\Delta b)^2}{\langle b^2\rangle} S_{CC}(Q) \tag{1}$$

where $\langle b\rangle = \sum_{i=T,Al} c_i\, b_i$, $\langle b^2\rangle = \sum_{i=T,Al} c_i\, b_i^2$ and $\Delta b = b_T - b_{Al}$ (T = Mn, $\sigma$-FeCr) $c_T$ and $b_T$ are the average atomic concentration and the average coherent scattering length of transition metal atoms ; $c_{Al}$ and $b_{Al}$ for Al atoms.

$$I(Q) = \left[\frac{d\sigma_{coh}}{d\Omega}(Q) - (\langle b^2\rangle - \langle b\rangle^2)\right]/\langle b\rangle^2 = \sum_{ij=T,Al} W_{ij}\, I_{ij}(Q)$$

$$I(Q) = \frac{c_T^2\, b_T^2}{\langle b\rangle^2} I_{TT}(Q) + \frac{c_{Al}^2\, b_{Al}^2}{\langle b\rangle^2} I_{AlAl}(Q) + \frac{2\, c_T\, c_{Al}\, b_T\, b_{Al}}{\langle b\rangle^2} I_{TAl}(Q) \tag{2}$$

$S(Q)$ and $I(Q)$ are two definitions of the total structure factor. In the following we will use preferentially the function $S(Q)$ which remains defined even for a zero alloy (i.e., when $\langle b\rangle = 0$).

For a liquid mixture, in the long wavelength ($Q \to 0$) limit, the number-concentration structure factors $S_{N,C}(Q)$ are related to the thermodynamic quantities following statistical mechanics [6] :

$$\begin{aligned} S_{NN}(0) &= \rho k_B\, TK_T + \delta^2 c_T\, c_{Al}\, S_{CC}(0) \\ S_{NC}(0) &= -\, c_T\, c_{Al}\, \delta S_{CC}(0) \\ S_{CC}(0) &= \mathcal{N} k_B\, T/c_T\, c_{Al} \left(\frac{\partial^2 G}{\partial c_T^2}\right)_{T,P} \end{aligned} \tag{3}$$

where $\rho$ is the atomic number density, $K_T$ the isothermal compressibility, $G$ the Gibbs free energy per mole, $k_B$ the Boltzmann constant, $\mathcal{N}$ the Avogadro number and $\delta$ is a dilatation factor defined by :

$$\delta = \frac{1}{V}\left(\frac{\partial V}{\partial c_T}\right)_{T,P}, \quad V \text{ being the molar volume of the mixture .}$$

From relations (1) and (3), the limit at $Q = 0$ of the total structure factor is given by :

$$S(0) = \frac{\langle b \rangle^2}{\langle b^2 \rangle} \rho k_B T K_T + \frac{(\langle b \rangle \delta - \Delta b)^2}{\langle b^2 \rangle} c_T c_{Al} S_{CC}(0) . \quad (4)$$

Using the linear relations between $I_{ij}(Q)$ and $S_{N,C}(Q)$ established by Bhatia and Thornton [6], the long wavelength limits of the Faber-Ziman PSFS are defined by :

$$\begin{aligned} I_{TT}(0) &= \phi - c_{Al}/c_T + c_{Al} c_T S_{CC}(0) \times (\delta - 1/c_T)^2 \\ I_{AlAl}(0) &= \phi - c_T/c_{Al} + c_{Al} c_T S_{CC}(0) \times (\delta + 1/c_{Al})^2 \\ I_{TAl}(0) &= \phi + 1 + c_{Al} c_T S_{CC}(0) \times (\delta - 1/c_T)(\delta + 1/c_{Al}) \end{aligned} \quad (5)$$

where $\phi$ is the product $\rho k_B T K_T$.

The paper is arranged as follows : in section 2, the characteristics of the pseudo-binary liquid alloys $(x, b_T)$ will be given, then the experimental and data analysis will be detailed. Particular attention will be paid to the determination of the long wavelength limit of $S(Q)$ which allows us to estimate the magnetic moment of transition metal atoms and the paramagnetic scattering correction. In section 3, the total structure factors, the Faber-Ziman and Bhatia-Thornton PSFs will be presented as well as their respective Fourier transforms. Finally, in section 4 given the average interactomic distances and partial coordination numbers, a comparison between the local orders in the liquid, quasicrystalline and crystalline phases will be attempted.

## 2. Experimental technique and data analysis.

Four cylindrical samples of $Al_{80}(Mn_x(FeCr)_{1-x})_{20}$ alloys with $x = 1$, 0.639, 0.304 and 0 were prepared, about 5.8 mm in diameter and 65 high. The largest contrast in neutron diffraction is obtained between the $Al_{80}Mn_{20}$ and $Al_{80}(FeCr)_{20}$ alloys ; the coherent scattering lengths of Mn atoms and the (FeCr) mixture which are of opposite signs are equal to $-0.373 \times 10^{-12}$ cm and $0.659 \times 10^{-12}$ cm, respectively. For $x = 0.639$, the alloy is characterized by an average transition metal atom coherent scattering length (noted $b_T$) which is equal to zero ; therefore the measurement of its structure factor yields directly the partial structure function $I_{AlAl}$ (see Eq. (2)). The composition of the fourth alloy ($x = 0.304$) was chosen so that $b_T$ became equal to the coherent scattering length of Al atoms, giving directly the number-number structure factor $S_{NN}$ (see Eq. (1)).

For these four studied alloys, the contributions of the partial function $S_{N,C}(Q)$ or $I_{ij}(q)$ to the total structure factors are given by the weights $W_{NC}$ or $W_{ij}$ listed in table I.

Table I. — *Weights of the partial functions defined in equations* (1) *and* (2). (T = Mn, $\sigma$-Fe-Cr ).

| Alloy | $W_{NN}$ | $W_{NC}$ | $W_{CC}$ | $W_{TT}$ | $W_{TAl}$ | $W_{AlAl}$ |
|---|---|---|---|---|---|---|
| $Al_{80}Mn_{20}$ | 0.33 | − 2.35 | 0.67 | 0.137 | − 1.015 | 1.878 |
| $Al_{80}(Mn_{0.639}(FeCr)_{0.361})_{20}$ | 0.8 | − 2 | 0.2 | 0 | 0 | 1 |
| $Al_{80}(Mn_{0.304}(FeCr)_{0.696})_{20}$ | 1 | 0 | 0 | 0.04 | 0.32 | 0.64 |
| $Al_{80}(FeCr)_{20}$ | 0.913 | 1.407 | 0.087 | 0.104 | 0.437 | 0.458 |

The atomic density of the liquid $Al_{80}(Mn_x(FeCr)_{1-x})_{20}$ alloys was estimated as 0.058 at/Å$^3$ from the density measurements of liquid AlCr and AlFe [8].

2.1 NEUTRON DIFFRACTION MEASUREMENTS. — The neutron diffraction measurements were carried out on the D4B diffractometer at the Institut Laue Langevin (Grenoble) using a wavelength of 0.705 Å. Cylindrical ingots of alloys were melted into sapphire cells of 1 mm wall thickness and 8 mm outside diameter, inside a furnace made of a vanadium heater (0.1 mm wall thickness, 28 mm diameter), placed at the center of the D4B vacuum chamber. For each composition, the intensity scattered either by the empty cell or by the empty cell plus the molten alloy was measured at the same temperature, chosen 100 K above the melting point ($T$ = 1 325, 1 370, 1 395 and 1 420 K for $x$ = 1, 0.639, 0.304 and 0 respectively). Each cell was previously orientated at room temperature in order to avoid the intense Bragg reflections. The height of the irradiated molten alloys was 50 mm. The diffracted intensities were measured by two $^3$He detectors of 64 cells each. The 2 $\theta$ scattering angles covered by the two detectors are for detector 1 located at 1.50 m from the sample : $2\theta_{min} = 1.6°$, $2\theta_{max} = 64.7°$ with an angular path of 0.1° per cell and for detector 2 at 0.75 m : $2\theta_{min} = 46.8°$, $2\theta_{max} = 131.4°$ with a path of 0.2°, allowing us to investigate a $Q$-range ($Q = 4\pi \sin\theta/\lambda$) from 0.27 to 16.26 Å$^{-1}$.

2.2 DATA ANALYSIS. — For each detector, corrections for the background, the furnace and cell scattering and for the sample self-absorption are applied. At low scattering angles ($2\theta < 2\theta_{min}^{Cd}$) the background intensity, $I_B(2\theta)$ is corrected for the sample transmission by measuring the intensity, $I_{Cd}(2\theta)$, obtained with an absorber (here a cadmium rod of the same diameter than that of the cell) positioned in the center of the vacuum chamber [9]. The intrinsic sample scattering $I_s(2\theta)$ is calculated from the measured intensities $I_{SCFB}(2\theta)$, $I_{CFB}(2\theta)$ and $I_{FB}(2\theta)$ (where S = sample, C = container, F = furnace and B = background) as follows :

For $2\theta < 2\theta_{min}^{Cd}$ (only for detector 1) :

$$I_S(2\theta) = A_1[I_{SCFB}(2\theta) - A_2(2\theta)\, I_{CFB}(2\theta) - A_3(2\theta)\, I_{FB}(2\theta) - (1 - A_2(2\theta) - A_3(2\theta))\, A_{HH}(2\theta)\, I_{Cd}(2\theta)]. \quad (7a)$$

For $2\theta > 2\theta_{min}^{Cd}$

$$I_S(2\theta) = A_1[I_{SCFB}(2\theta) - A_2(2\theta)\, I_{CFB}(2\theta) - A_3(2\theta)\, I_{FB}(2\theta) - (1 - A_2(2\theta) - A_3(2\theta))\, A_{HH}(2\theta)\, I_B(2\theta)]. \quad (7b)$$

Above $2\theta_{min}^{Cd}$, $I_{Cd}$ is higher than $I_B(2\theta)$ due to scattering of the cadmium. The absorption factors $A_i(2\theta)$ and $A_{HH}(2\theta)$ are calculated using the expressions [10] deriving from the formalism of Paalman and Pings [11] extended to two coaxial cylinders. The corrected sample intensities of both detectors are then regrouped using the overlapping angular range. Finally the intrinsic sample scattering is corrected for the isotropic multiple scattering estimated as in [12], for the inelastic scattering by the method of Yarnell *et al.* [13] and for the incoherent scattering of the pseudo-binary alloy which may be written as :

$$\sigma_{incoh}(\text{alloy}) = 0.8\, \sigma_{incoh,\,Al} + 0.2\, \sigma_{incoh,\,T}(x)$$

$\sigma_{incoh,\,T}(x)$ is the incoherent cross-section of transition metal atoms in the alloy given by :

$$\sigma_{incoh,\,T}(x) = 4\pi[\langle b_j^2\rangle - b_T^2] + [x\sigma_{incoh,\,Mn} + (1-x)(0.5\, \sigma_{incoh,\,Fe} + 0.5\, \sigma_{incoh,\,Cr})] \quad (8)$$

and

$$\langle b_j^2\rangle = x b_{Mn}^2 + (1-x)\, 0.5\, (b_{Fe}^2 + b_{Cr}^2).$$

The first term of equation (8) represents the incoherent scattering due to the mixture of the Mn, Fe and Cr atoms, and the second term is the contribution from isotope and spin incoherence of each species. The calculation of $\sigma_{\text{incoh, T}}(x)$ from equation (8) is simpler than that proposed for the structural study of the amorphous $(Fe_xMn_{1-x})_{35}Y_{65}$ alloy [14]. From the coherent scattering lengths and the incoherent scattering cross sections of elements given in table II, the values of $\sigma_{\text{incoh, T}}(x)$ are equal to 2.21, 4.49 and 4.14 barns for $x = 0$, 0.304 and 0.639 respectively.

Table II. — *Coherent scattering lengths, incoherent scattering cross sections and absorption cross-sections for* $\lambda = 0.705$ Å [15, 16].

| | Al | Cr | Mn | Fe |
|---|---|---|---|---|
| $b_{\text{coh}}$ $(10^{-12}\text{ cm})$ | 0.3449 | 0.3635 | − 0.373 | 0.954 |
| $\sigma_{\text{incoh}}(b)$ | 0.0085 | 1.80 | 0.402 | 0.41 |
| $\sigma_{\text{abs}}(b)$ | 0.09 | 1.202 | 5.208 | 0.995 |

The normalisation constant, $C_0$, is estimated at high $Q$ values on an interval $[Q_i, Q_j]$ in which the amplitudes of the oscillations of $I_S(Q)$ are weak [17], such as :

$$C_0 = \sum_{Q_i}^{Q_j} I_S(Q) / \sum_{Q_i}^{Q_j} \frac{d\sigma^\infty}{d\Omega}(Q)$$

and

$$\frac{d\sigma^\infty}{d\Omega}(Q) = \sum_{i=T,Al} c_i(b_i^2 + \sigma_{\text{incoh, i}}/4\pi) + \frac{d\sigma_{\text{mult}}}{d\Omega} + \frac{d\sigma_{\text{inel}}}{d\Omega}(Q).$$

In the expression of $(d\sigma^\infty/d\Omega)(Q)$ the interference effects are neglected. $d\sigma_{\text{mult}}/d\Omega$ and $(d\sigma_{\text{inel}}/d\Omega)(Q)$ are the multiple and inelastic scattering cross-sections per atom.

The coherent scattering cross-section per atom is then given by :

$$\frac{d\sigma_{\text{coh}}}{d\Omega}(Q) = \frac{I_S(Q)}{C_0} - \sum_{i=T,Al} c_i\,\sigma_{\text{incoh, i}}/4\pi - \frac{d\sigma_{\text{mult}}}{d\Omega} - \frac{d\sigma_{\text{inel}}}{d\Omega}(Q). \quad (9)$$

However, for the four alloys, (i) the low $Q$ value of the total structure factor $S^T(Q) = (d\sigma_{\text{coh}}/d\Omega)(Q)/\langle b^2\rangle$ deduced from equation (9) are much higher than the expected long wavelength limit $S(0)$ using the following thermodynamic quantities in equation (4) : $K_T = 1.85 \times 10^{-11}\text{ N}^{-1}\text{ m}^2$ [18], $\delta = -0.6$ [8] and $S_{CC}(0) = 0.5$ ; $S_{CC}(0)$ being deduced from the activity measurements of aluminium in liquid AlFe alloys [19]-[21] and in liquid AlCr alloys [22]

(see Tab. III). As a matter of fact, by assuming that below 0.275 $\text{Å}^{-1}$ the signal is flat, $S^T(0.275)$ and $S(0)$ should be identical. Moreover (ii), the Fourier transform of $S^T(Q)$ exhibits at low $r$ values a composition dependent positive oscillation. The inverse Fourier transform of this oscillation is a continuously decreasing function with $Q$ which becomes zero around 7 $\text{Å}^{-1}$. These two points indicate that the transition metal atoms give rise to a paramagnetic scattering for which we must correct our measurements. The paramagnetic scattering cross-section is described by [23] :

$$\frac{d\sigma_{\text{pm}}}{d\Omega}(Q) = \frac{2}{3}\left(\frac{e^2\gamma}{mc^2}\right)^2 S(S+1)\,f_T^2(Q) \quad (10)$$

Table III. — *Low Q value of the measured total structure factor (Eq. (9)), $S^T(0.275)$, calculated long wavelength limit, $S(0)$, and effective Bohr magneton number per T atom, $\mu_{eff}$, deduced from the difference $S^T(0.275) - S(0)$ (see text).*

| Alloy | $S^T(0.275)$ | $S(0)$ | $\mu_{eff}$ |
|---|---|---|---|
| $Al_{80}Mn_{20}$ | 0.892 | 0.238 | 2.88 |
| $Al_{80}(Mn_{0.639}(FeCr)_{0.361})_{20}$ | 0.782 | 0.043 | 2.69 |
| $Al_{80}(Mn_{0.304}(FeCr)_{0.696})_{20}$ | 0.505 | 0.049 | 2.37 |
| $Al_{80}(FeCr)_{20}$ | 0.330 | 0.157 | 1.8 |

where $m$ is the electron mass, $e$ the charge, $c$ the velocity of light and $\gamma$ the neutron magnetic moment. $S$ is the spin quantum number of transition metal atoms, and $f_T(Q)$ their amplitude form factor. Here, we use the fonction $f_T(Q)$ calculated for Mn atoms which is similar to those for Fe and Cr atoms [24]. Finally the total structure factor corrected for the paramagnetic scattering weighted by the concentration of T atoms is given by :

$$S(Q) = \left( \frac{I_S(Q)}{C_0} - \sum_{i=T,Al} c_i(\sigma_{incoh,i}/4\pi) - \frac{d\sigma_{mult}}{d\Omega} - \frac{d\sigma_{inel}}{d\Omega}(Q) - 0.2\frac{d\sigma_{pm}}{d\Omega}(Q) \right) / \langle b^2 \rangle . \quad (11)$$

Since the contribution of $(d\sigma_{pm}/d\Omega)(Q)$ is negligible at high $Q$-values, the normalisation constant $C_0$ is identical in equations (10) and (11). Consequently, for each alloy, the product $S(S+1)$ can be deduced from the difference $S^T(0.275) - S(0)$ with $f_T(0) = 1$. In table III, we list the average effective Bohr magneton numbers, $\mu_{eff} = 2\sqrt{S(S+1)}$. $\mu_{eff}$ decreases with replacing Mn atoms by the FeCr mixture but remains larger in the liquid phase than in the icosahedral phase $Al_{80}Mn_{20}$ for which an effective moment of 1.1 $\mu_B$ was obtained from magnetic susceptibility measurements [25]. Therefore, the estimated $\mu_{eff}$ values in the liquid alloys must be taken with care, because the paramagnetic scattering correction, as applied above, could include other scattering effects such as : multiple cross scattering effects between container and sample.

## 3. Results and discussion.

3.1 TOTAL STRUCTURE FACTORS AND PAIR DISTRIBUTION FUNCTIONS. — The total structure factors of the four alloys $Al_{80}(Mn_x(FeCr)_{1-x})_{20}$ deduced from equation (11) are shown in figure 1. At high $Q$-values, the signal produced by the sapphire cells was not fully reproducible since the difference between $I_{SCFB}(Q)$ and $I_{CFB}(Q)$ measured at the same temperature could not accurately correct some container Bragg peaks. As long as these perturbations of the signal were restricted to very narrow ranges, they could be corrected for by data smoothing. However beyond 13.7 $Å^{-1}$, this correction was no more possible. For future measurements, it will be important to stabilize the cells after machining by annealing them at higher temperatures ($\simeq$ 1 600 K). With decreasing Mn content, the first peak of $S(Q)$ shifts towards higher $Q$ and its intensity increases : the peak positions $Q_1$ are 2.52, 2.83, 2.85 and 2.89 $Å^{-1}$ for $x = 1$, 0.639, 0.304 and 0 respectively. The bump at 1.6 $Å^{-1}$ observed in the $S(Q)$ of $Al_{80}(FeCr)_{20}$ and especially the strong shoulder at the left-side of the first peak of $Al_{80}Mn_{20}$ indicates a chemical ordering between Al and T atoms.

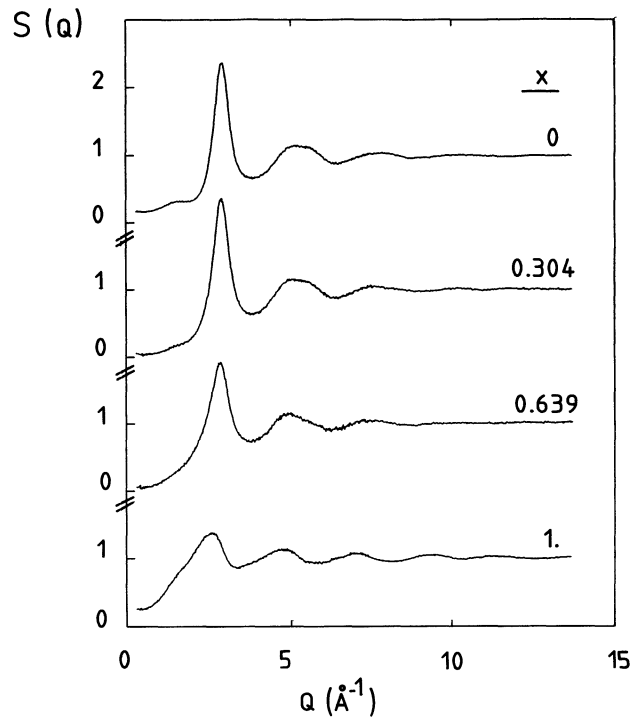


Fig. 1. — Total structure factors of the liquid $Al_{80}(Mn_x(FeCr)_{1-x})_{20}$ alloys.

Figure 2 shows the Fourier transform of $Q(S(Q)-1)$, the reduced atomic distribution function $G(r)$ :

$$G(r) = \frac{2}{\pi} \int_{Q_{min}}^{Q_{max}} Q(S(Q)-1) \sin Qr \, dQ \, . \tag{12}$$

The $G(r)$ curves are calculated with truncation values, $Q_{max}$ equal to 13.45, 12.65, 13.7 and 13.7 Å$^{-1}$ for $x = 1$, 0.639, 0.304 and 0, respectively and $Q_{min}$ equal to 0.275 Å$^{-1}$ for any $x$. The first relevant peak in the $G(r)$ function of $Al_{80}Mn_{20}$ is negative and located at around 2.5 Å ; from table I it describes the distribution of the nearest neighbor AlT pairs. Beyond its first positive peak at 2.9 Å, its oscillations damp rapidly down. With decreasing Mn content, the first peak shifts towards smaller distances up to 2.66 Å for $x = 0$, in great part due to the decrease of the AlAl pair contribution for the benefit of the TAl pair contribution.

### 3.2 Partial structure factors and partial correlation functions.

3.2.1 *Bhatia-Thornton formalism.* — The Bhatia-Thornton PSFs are derived by solving the best conditioned system formed by the three measured $S(Q)$'s for $x = 1$, 0.639 and 0 (Eq. (1)). The accuracy is around 2 % for $S_{NN}$, 1 % for $S_{NC}$ and 7 % for $S_{CC}$ ; beyond 7.5 Å$^{-1}$, due to the higher counting rate at the detector 2 position, the accuracy is even better as it can be seen from the noise on the curves shown in figure 3. The first and second peaks of the $S_{NN}$ function are identical to those of the total structure factor of $Al_{80}(Mn_{0.304}(FeCr)_{0.696})_{20}$. This confirms well the isomorphous behaviour between Mn atoms and the FeCr mixture in the liquid state. Beyond the third peak, a detailed analysis of the

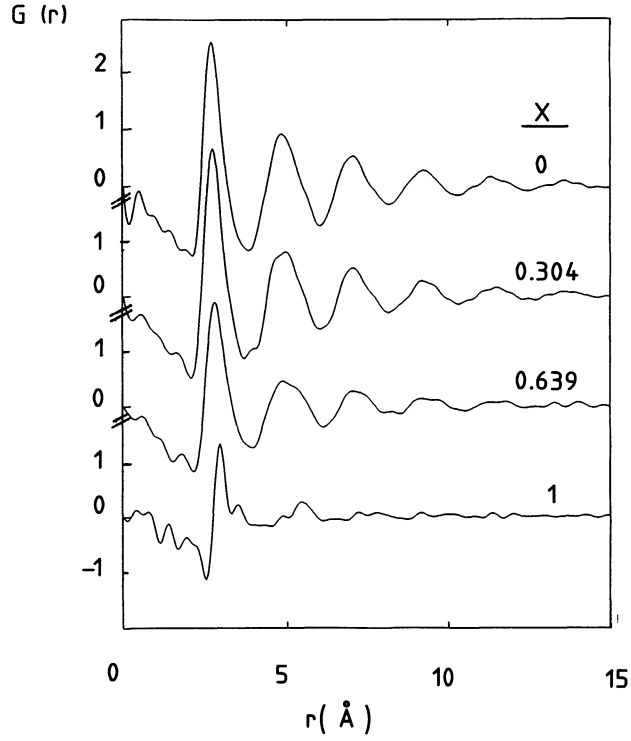


Fig. 2. — Reduced atomic distribution functions of the liquid $Al_{80}(Mn_x(FeCr)_{1-x})_{20}$ alloys.

container correction for $Al_{80}(Mn_{0.304}(FeCr)_{0.696})_{20}$ shows that the substantial differences observed can be explained by a reduction of stresses in the cell during its measurement. The $S_{NN}$ function exhibits two striking features : 1) a narrow first peak located at 2.85 $Å^{-1}$, from its width ($\Delta Q^1_{NN}$) a correlation length of 10 Å can be calculated according to the formula $\xi_T = 2\pi/\Delta Q^1_{NN}$ showing the existence of medium range topological order ; 2) a shoulder on the right side of its second peak. This feature commonly observed for metallic glasses was also evidenced in the liquid $Mg_{70}Zn_{30}$ alloy, but less pronounced than in the amorphous state [26, 27]. We have indicated by arrows the two distinct peak positions which are suggestive of short range icosahedral order [28], defined from the first peak position $Q_1$ by $Q_{2a} = 1.7\,Q_1$ and $Q_{2b} = 2\,Q_1$. Note that $Q_{2b}$ matches quite well the position of the experimental shoulder.

By contrast, the first peak of $S_{CC}(Q)$ centered around 2.1 $Å^{-1}$, is broad and of rather low intensity, reflecting a weak chemical ordering. Its width yields a short chemical ordering correlation length of about 4 Å. Up to now the function $S_{CC}$ has been determined only for a few liquid systems, such as the Li-based liquids and it appears that the $S_{CC}$ function of the $Al_{80}T_{20}$ liquid is quite comparable to that of $Al_{28}Li_{72}$ [29].

The number concentration structure factor exhibits one defined oscillation of weak amplitude ($Q_1^{min} = 2.40$ $Å^{-1}$, $S(Q^{min}) = -0.1$ and $Q_1^{max} = 2.95$ $Å^{-1}$, $S(Q_1^{max}) = 0.12$), reflecting the relatively small size effect between the two species. It is worth noting that the $S_{NC}$ function calculated by the hard sphere model in the Percus Yevick approximation (dotted curve in Fig. 3) does not fit the experimental curve. In particular, the amplitude of the first oscillation is underestimated even when we choose the largest possible ratio of hard sphere diameters of our pseudo-binary system obtained by comparing Fe and Al atoms. This ratio is

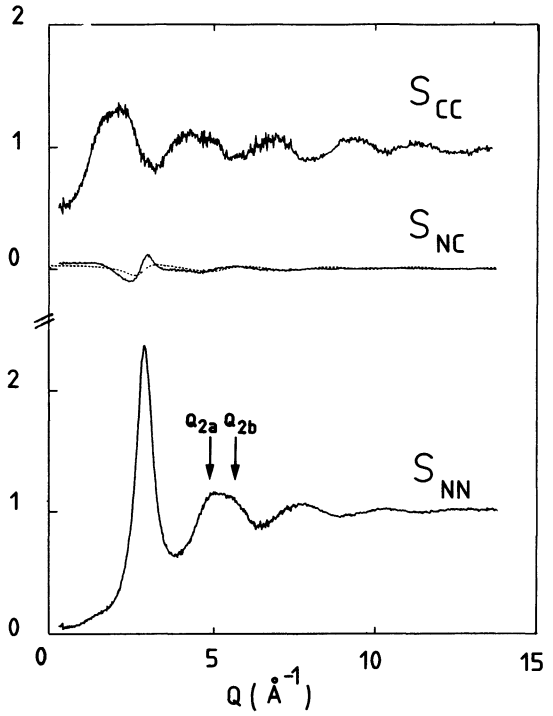


Fig. 3. — Bhatia-Thornton partial structure factors of the liquid $Al_{80}(Mn_x(FeCr)_{1-x})_{20}$ alloys. For $S_{NC}$ the dotted curve is obtained by the hard sphere model with hard sphere diameters of 2.47 Å and 2.26 Å for Al and T atoms respectively. $Q_{2a}$ and $Q_{2b}$ are the two peak positions suggestive of short range icosahedral order [28], defined from the first peak position $Q_1$ ($Q_{2a} = 1.7\ Q_1$, $Q_{2b} = 2\ Q_1$).

calculated from the experimental entropies of pure liquids at their respective melting points (i.e., $\sigma_{Fe} = 2.26$ Å at 1 809 K and $\sigma_{Al} = 2.47$ Å at 933 K yielding a packing fraction of the alloy $\eta$ equal to 0.435, while $\sigma_{Mn} = 2.32$ Å at 1 517 K with $\eta$ equal to 0.44). An explanation of this disagreement will be proposed in the next paragraph from the nearest-neighbor distances between like and unlike atoms. The values of $S_{NN}(Q)$, $S_{NC}(Q)$ and $S_{CC}(Q)$ at the first measurable momentum transfer, $Q = 0.275$ Å$^{-1}$, equal to 0.056, 0.046 and 0.501 are quite close to the long wavelength limits calculated at an average temperature of 1 400 K from equation (3) (i.e. $S_{NN}(0) = 0.049$, $S_{NC}(0) = 0.048$ and $S_{CC}(0) = 0.5$, as obtained from the thermodynamic quantities given in paragraph 2.2).

Figure 4 shows the three number concentration correlation functions $G_{NN}$,$G_{NC}$ and $G_{CC}$ obtained by Fourier transformation of the $S_{N,C}(Q)$'s with optimised truncation values equal to 13.7, 8.15 and 9.9 Å$^{-1}$ respectively. The first four peaks of $G_{NN}$ centered at 2.65, 4.82, 7 and 9.3 Å are well defined, indicating that the topological ordering extends over several interatomic distances. The $G_{CC}$ function presents a negative peak at 2.50 Å associated to the first unlike atom distances, followed by two small positive peaks centered around 2.95 and 3.65 Å. Beyond 4 Å, the absence of significant peaks is entirely in agreement with the correlation length calculated above. Some deviation of the oscillations of $S_{CC}$ around 1 can explain the spurious ripples observed under 2.5 Å in $G_{CC}$.

3.2.2 *Faber-Ziman formalism.* — The Faber-Ziman PSFs are determined from the three measured $I(Q)$'s for $x = 1$, 0.639 and 0 (Eq. (2)). From the curves shown in figure 5, it can be

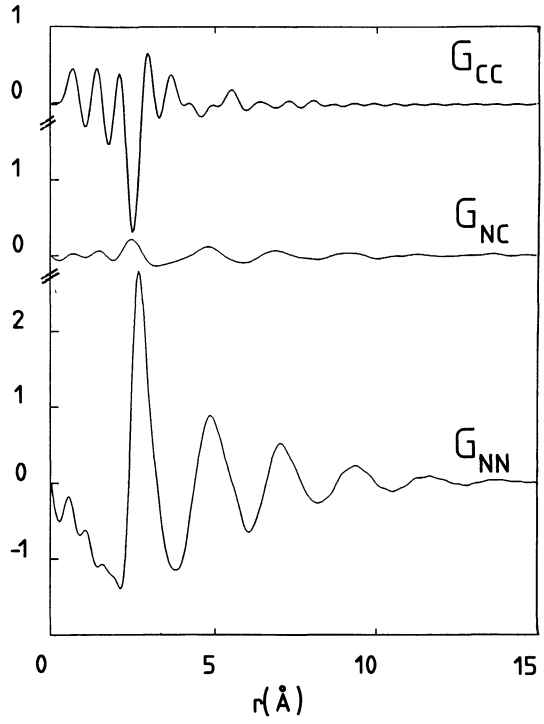


Fig. 4. — Number concentration correlation functions of the liquid $Al_{80}(Mn_x(FeCr)_{1-x})_{20}$.

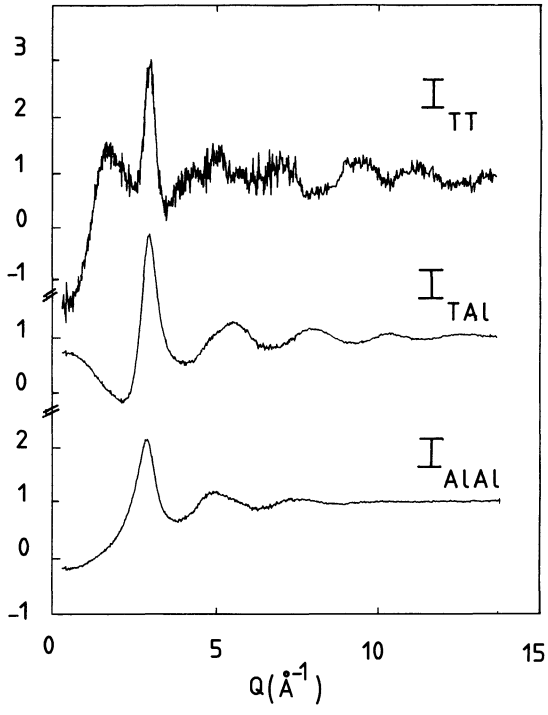


Fig. 5. — Faber-Ziman partial structure factors of the liquid $Al_{80}(Mn_x(FeCr)_{1-x})_{20}$ : T = Mn or $\sigma$-FeCr.

observed that the accuracy is very good on the partial functions $I_{TAl}$ and $I_{AlAl}$ (about 2-3 %) and rather average on the partial function $I_{TT}$, relative to the minority atom pairs (20 %). We report in table IV, the peak positions and the intensities of $I_{ij}(Q)$, their low $Q$ values, as also their thermodynamic limits calculated by equations (5).

As foreseen from the data analysis procedure, the low $Q$ values ($Q = 0.275$ Å$^{-1}$) are equal to the thermodynamic limits. Their signs, negative for like atom pairs and positive for unlike atom pairs, confirm the existence of a chemical ordering, also shown by the prepeak in $I_{TT}$ and the preminimum in $I_{TAl}$. It is important to emphasize that the function $I_{TT}$ presents a first peak which is narrower and higher than those of the two other functions and that the amplitudes of its oscillations remain quite large up to 13 Å$^{-1}$. Note also the small structures of its second oscillation. By contrast, the oscillations of $I_{AlAl}$ damp down rapidly ; this can be attributed to the softness of the repulsive part of the AlAl pair potential.

Table IV. — *Long wavelength limits $I_{ij}(0)$ and main features of the $I_{ij}(Q)$ functions (peak positions in Å$^{-1}$ units and intensities in brackets), for the liquid $Al_{80}(Mn_x(FeCr)_{1-x})_{20}$ alloys.*

| Function | $I_{ij}(0)$ | $I_{ij}(0.275)$ | Prepeak or preminimum | First peak | Second peak |
|---|---|---|---|---|---|
| | | | 1.65 | 2.9 | ≃ 5 |
| $I_{TT}$ | (– 1.47) | (– 1.48) | (1.55) | (2.95) | (1.5) |
| | | | 2.1 | 2.87 | 5.45 |
| $I_{TAl}$ | (0.729) | (0.727) | (– 0.19) | (2.85) | (1.28) |
| | | | | 2.83 | 4.9 |
| $I_{AlAl}$ | (– 0.195) | (– 0.183) | | (2.14) | (1.2) |

The reduced partial pair correlation functions, $G_{ij}(r)$ obtained by Fourier transformation of $Q(I_{ij}(Q) - 1)$ are shown in figure 6. The optimized truncation values used are 7.4, 10.75 and 12.6 Å$^{-1}$ respectively for $G_{TT}$, $G_{TAl}$ and $G_{AlAl}$. For comparison, we also show the function $G_{TT}$ calculated with a higher truncation value of 9.9 Å$^{-1}$ (dashed curve, Fig. 6). We see that by taking a smaller truncation value the spurious ripples especially at small $r$ are considerably reduced and the resolution of the first peak is decreased. But the number of TT nearest neighbor pairs deduced from the area under the first peak is unchanged. Thus the comparison of both curves of $G_{TT}$ allows principally to separate the relevant peaks of the TT pair distribution from the unrelevant ones. While the first peak of $G_{TT}$ is symmetric, it is asymmetric for $G_{TAl}$ and $G_{AlAl}$ ; for $G_{TAl}$ this asymmetry arises from the existence of a shoulder around 3.1 Å. Beyond the first neighbors, the MnMn and MnAl correlations are better defined than the AlAl ones.

From the first neighbor distances equal to 2.56, 2.74 and 2.89 Å for the pairs TAl, AlAl and TT respectively, it is worth noting that the first distance between unlike atoms is smaller than those between like atoms. The latter ones are rather different from those measured in the pure liquids near the melting point (i.e. 2.82 Å in Al, 2.67 Å in Mn and 2.58 Å in Fe or Cr [30]). In particular, the first distance TT is longer than the average distance in Mn and Fe (or Cr) liquids of 2.62 Å, indicating that the T atoms are not in close contact ; this suggests that the T atoms are arranged in order to respect a well-defined topological order. These figures can also explain why the function $S_{NC}(Q)$ is not well fitted by a mixture of hard spheres. In other respects, the first distance TAl smaller than the sum of the metallic atomic radii of the

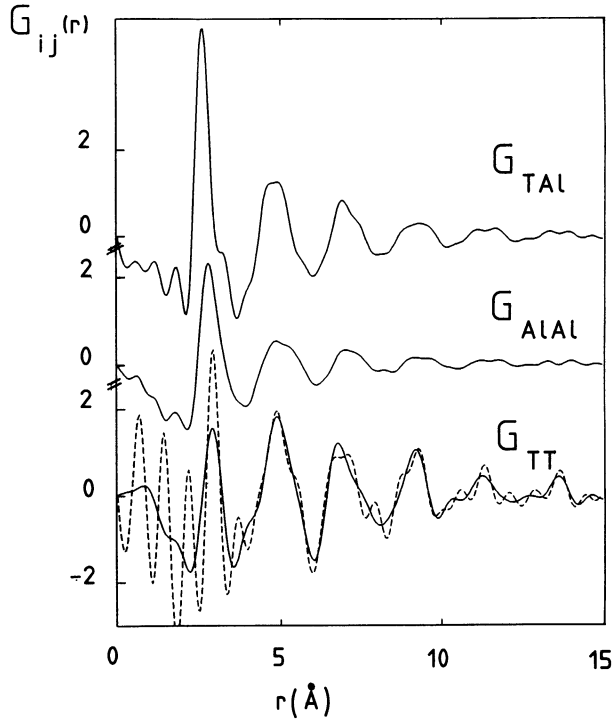


Fig. 6. — Reduced partial pair correlation functions of the liquid $Al_{80}(Mn_x(FeCr)_{1-x})_{20}$. The $G_{TT}$ curves are obtained by Fourier transformation of $Q\ (I_{TT}(Q) - 1)$ with truncation values equal to 7.4 $Å^{-1}$ (full curve) and 9.9 $Å^{-1}$ (dashed curve).

pure elements (with a ligancy of 12, $r_{Al} = 1.43$ Å and $r_T = 1.3$ Å) is an indication of chemical interactions associated with the sp-d hybridization.

3.3 PARTIAL COORDINATION NUMBERS AND CHEMICAL SHORT RANGE ORDER PARAMETER. — By integration of the peaks of the partial radial distribution functions $RDF_{ij}(r)$ we obtain the partial coordination numbers in the different coordination shells as follows :

$$z_{ij}^1 = c_j \int_{r_{ij,\,min}^1}^{r_{ij,\,max}^1} RDF_{ij}(r)\, dr \qquad (13)$$

where $r_{ij,\,min}^1$ and $r_{ij,\,max}^1$ are the lower and upper limits of the shell defined by the minima in $RDF_{ij}$.

$RDF_{ij}$ is related to $G_{ij}(r)$ by :

$$RDF_{ij}(r) = rG_{ij}(r) + 4\,\pi r^2 \rho\ .$$

In table V are reported the interatomic distances and the partial coordination numbers in the $Al_{80}T_{20}$ liquids, as also those found by neutron diffraction in the icosahedral, decagonal and the hexagonal phases of close composition [3, 4]. We will return to a detailed comparison in the next paragraph.

A method of evaluating the chemical ordering effects is to calculate the Warren chemical short-range order parameter generalized by Wagner and Ruppersbserg [31]. We recall the

definition of $\alpha_1$ and its normalised value $\alpha_1$ with regard to the maximum order parameter obtained when $z^1_{TAl} = z^1_T$ :

$$\alpha_1 = 1 - z^1_{TAl}/c_{Al}(c_T z^1_{Al} + c_{Al} z^1_T)$$

with

$$z^1_i = z^1_{ii} + z^1_{ij} \quad (i, j = T, Al)$$

and

$$\alpha_1 = \alpha_1/\alpha_1^{max} \quad \text{and} \quad \alpha_1^{max} = 1 - z^1_T/c_{Al}(c_T z^1_{Al} + c_{Al} z^1_T) .$$

Using the coordination numbers listed in table V, $\alpha_1$ is equal to $-0.05$ and $\alpha_1^0$ to 0.23 (with $\alpha_1^{max} = -0.214$). If we choose, now, for all pairs the same upper limit of the first coordination shell in integral 13 (defined as the position of the first minimum of $G_{NN}$ at 3.75 Å), as we did for the binary amorphous alloys exhibiting a large size effect [14], $\alpha_1$ and $\alpha_1^0$ become equal to $-0.057$ and 0.24, i.e. nearly as the previous values. This is consistent with the relatively small size effect in the $Al_{80}T_{20}$ liquids. Finally the negative value of $\alpha_1$ indicates a moderate chemical ordering.

## 4. Comparison of the local orders in the liquid, quasicrystalline and crystalline phases.

Since the $Al_{74}Si_5Mn_{21}$ icosahedral and $Al_{80}Mn_{20}$ decagonal phases can be produced by rapid quenching from the liquid state, it is worth comparing the local atomic arrangements in the liquid alloy with those in the quasicrystalline phases, and also in a crystalline phase which has a composition similar to the one of the icosahedral phase, namely the hexagonal $\beta$-$Al_9SiMn_3$ phase. This analysis is based on the experimental partial pair correlation functions shown in figure 7, which for the quasicrystalline and crystalline phases have been previously determined by neutron diffraction also using the isomorphous substitution between Mn atoms and the FeCr mixture [3, 4]. The main features deduced from these functions (interatomic distances and coordination numbers) are reported in table V.

By looking at the three series of curves (Figs. 7a.b.c.), it appears that whatever the state (liquid, quasicrystalline or crystalline) the correlations between the transition metal atoms (TT) are significantly defined further in real space than those between unlike atoms (TAl) ; the latter ones being also defined further than the correlations between Al atoms (for the liquid, this change is still more visible in the reduced pair distribution functions in Fig. 6). This behaviour shows that the topological order of the liquid cannot be simply described by a packing of hard spheres, as also indicated by the shape of the second peak of the $S_{NN}$ function impossible to represent with the hard sphere model.

In the following, we will show that by examining each series of atomic pair distribution function the local topological order of the liquid cannot be directly related to those of the quasicrystalline or $\beta$ phases.

Starting with the TT correlations, it appears that in the liquid the first TT distance is longer that those in the other phases and the number of first TT nearest neighbours is intermediate between those of the icosahedral and hexagonal phases (see Tab. V). A second difference is in the second pair distribution unsplitted up into two components. By contrast, the first AlAl distance is shortest in the liquid and the corresponding first neighbor number is slightly larger. Also, the higher AlAl distances are more spread out in the liquid, in comparison with the three components of the second pair distribution exhibited in the quasicrystalline phases.

Common features between the liquid and quasicrystalline phases can be really found in the unlike atom pair distribution : the same first TAl distance, the existence of a shoulder on the right hand side of the first peak in the liquid and icosahedral phases and close first

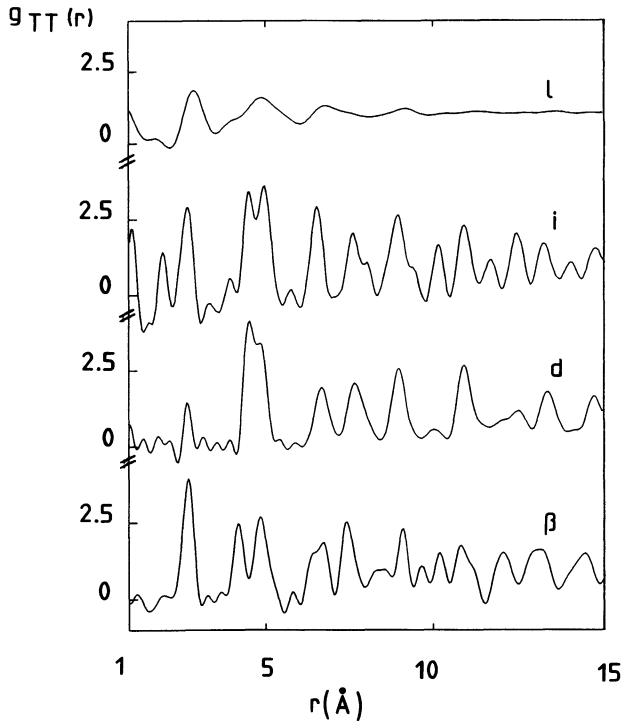


(a)

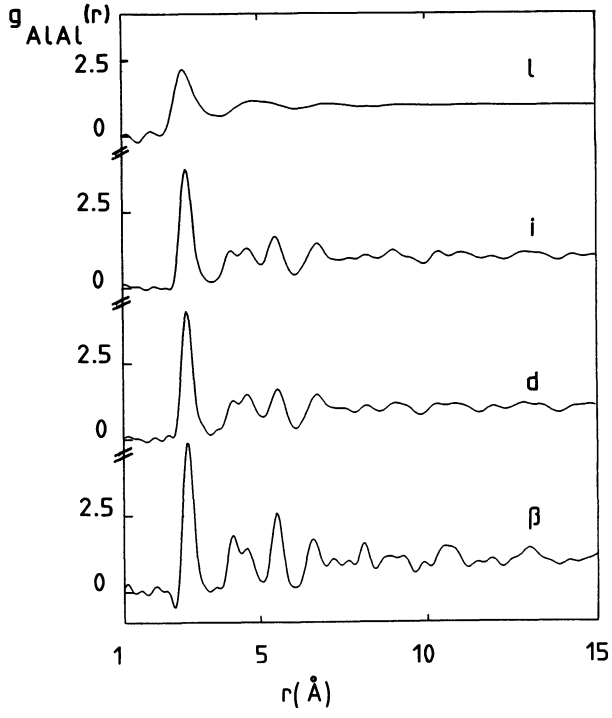


(b)

Fig. 7. — Partial pair correlation functions for the liquid $Al_{80}(Mn_x(FeCr)_{1-x})_{20}$ (l), icosahedral $Al_{74}Si_5Mn_{21}$ (i) [3], decagonal $Al_{80}Mn_{20}$ (d) [4] and hexagonal $\beta$-$Al_9SiMn_3$ ($\beta$) [3] phases : (a) $g_{TT}$ ; (b) $g_{AlAl}$ ; (c) $g_{TAl}$.

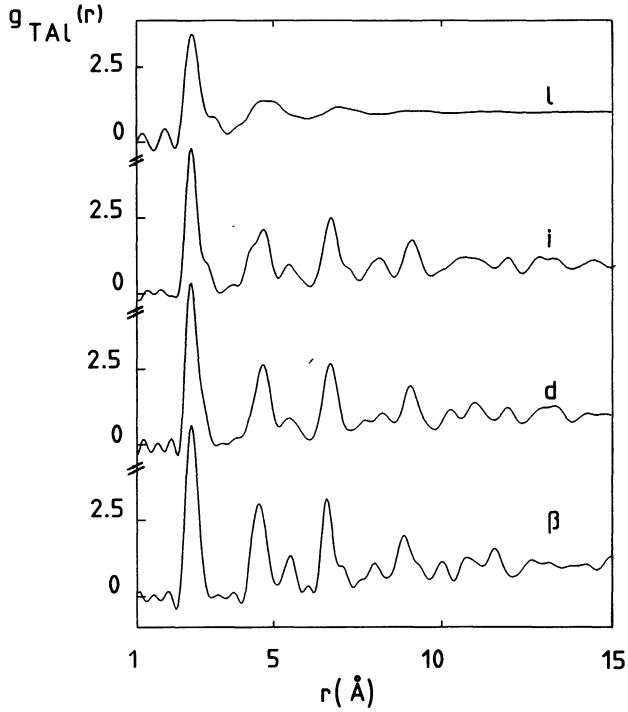


Fig. 7(c)

Table V. — *Interatomic distances and coordination numbers in the first and second shells for the liquid, quasicrystalline* [3, 4] *and β crystalline* [4] *phases.*

| | Liquid $Al_{80}T_{20}$ | | Icosahedral $Al_{74}Si_5Mn_{21}$ | | Decagonal $Al_{80}T_{20}$ | | β-phase $Al_9SiMn_3$ | |
|---|---|---|---|---|---|---|---|---|
| | $r_{ij}$ (Å) | $z_{ij}$ | $r_{ij}$ (Å) | $z_{ij}$ | $r_{ij}$ (Å) | $z_{ij}$ | $r_{ij}$ (Å) | $z_{ij}$ |
| | 2.89 | 1.5 | 2.7 | 0.75 | 2.6 | 0.3 | 2.67 | 2.2 |
| TT | 4.85 | 8.53 | 4.47 | 5.12 | 4.5 | 5.1 | 4.17 | 3.4 |
| | | | 4.93 | 6.67 | 4.8 | 4.8 | 4.8 | 5.8 |
| | 2.56 | 9.5 | 2.57 | 9.76 | 2.55 | 10.4 | 2.55 | 9.3 |
| TAl | 4.6 | 31.8 | 4.68 | 21.1 | 4.65 | 23 | 4.55 | 20 |
| | | | 5.43 | 11.5 | 5.4 | 10 | 5.47 | 11.9 |
| | 2.74 | 10.22 | 2.81 | 9.5 | 2.8 | 9.6 | 2.82 | 8.9 |
| AlAl | 4.8 | 32.7 | 4.15 | 16.6 | 4.2 | 6.3 | 4.15 | 7.5 |
| | 5.3 | | 4.63 | | 4.65 | 11.6 | 4.57 | 7.7 |
| | | | 5.45 | 20.4 | 5.5 | 20 | 5.47 | 19.5 |

coordination numbers. But it is believed that these common points result from the same chemical interactions rather than from the same type of topological order in the liquid and icosahedral phases. Once again, the second TAl distances are less ordered in the liquid.

In conclusion, it turns out that on the basis of isotropic regrouping in real space, the local topological order in the liquid, supported by both the TT correlations defined quite far in real space and the shape of the first two peaks of the $S_{NN}$ function, is different from those existing in the quasicrystalline phases or in the hexagonal phase topologically close to the icosahedral phase. Therefore, information on the bond-angle distributions, such as those determined in the simple metal liquid alloys [32], is really necessary to confirm the existence of a local icosahedral order in the liquid $Al_{80}Mn_{20}$ alloy.

**Acknowledgments.**

The authors are grateful to Professor P. Desre for stimulating this study and to the Institut Laue Langevin for allocation of beam time. Thanks are due to J. P. Houin for preparing the master ingots.

## References

[1] SHECHTMAN, D., BLECH, I., GRATIAS, D., CAHN, J. W., *Phys. Rev. Lett.* **53** (1984) 1951.
[2] JANOT, Ch., PANNETIER, J., DUBOIS, J. M., FRUCHART, R., *Phys. Lett.* **A119** (1986) 309.
[3] DUBOIS, J. M., DE BOISSIEU, M., ILL-CODEST Workshop on Quasicrystalline materials, Grenoble (March 1988) Eds. Ch. Janot and J. M. Dubois (World Scientific) p. 97.
[4] DUBOIS, J. M., JANOT, Ch., *Europhys. Lett.* **5** (1988) 235.
[5] STEINHARDT, J. P., NELSON, D. R., RONCHETTI, M., *Phys. Rev.* **B28** (1983) 784.
[6] BHATIA, A. B., THORNTON, D. E., *Phys. Rev. B* **2** (1970) 3004.
[7] FABER, T. E., ZIMAN, J. M., *Philos. Mag.* **11** (1965) 153.
[8] AJUSHINA, G. D., LEVIN, E. S., GEL'D, P. V., *J. Phys. Chem.* **42** (1968) 1489.
[9] BERTAGNOLLI, A., CHIEUX, P., ZEIDLER, M. D., *Mol. Phys.* **32** (1976) 759.
[10] PONCET, J. F., Thesis, University of Reading (1976).
[11] PAALMAN, H. H., PINGS, C. J., *J. Appl. Phys.* **33** (1962) 2635.
[12] BLECH, J. A., AVERBACH, B. L., *Phys. Rev. A.* **137** (1965) 1113.
[13] YARNELL, J. L., KATZ, M. J., WENZEL, R. G., KOENIG, S. H., *Phys. Rev. A* **7** (1973) 2130.
[14] MARET, M., PASTUREL, A., CHIEUX, P., *J. Phys. F. : Met. Phys.* **17** (1987) 2191.
[15] KOESTER, L., YELON, W. B., Neutron Diffraction Newsletter, Ed. by the Neutron Diffraction Commission of the International Union of Crystallography (1983).
[16] SEARS, V. F., Atomic Energy of Canada Limited Report, No. AECL-8490, Chalk-River (1984).
[17] BLETRY, J., Thèse d'Etat, Université de Grenoble (1979).
[18] TEKUCHEV, V. V., STREMOUSOV, V. I., *Zh. Fiz. Khim.* **59** (1985) 2258.
[19] MITANI, H., NAGAI, H., *Nippon Kinzoku Gakkaishi* **32** (1968) 752.
[20] COSKUN, A., ELLIOTT, J. F., *Trans. AIME* **242** (1968) 253.
[21] BELTON, G. R., FRUEMAN, R. J., *Trans. AIME* **245** (1969) 113.
[22] OFORKA, N. C., *Indian J. Chem.*, **25**A (1986) 263.
[23] BACON, G. E., Neutron Diffraction (Oxford University Press) 1985, p. 191.
[24] WATSON, R. E., FREEMAN, A. J., *Acta Cryst.* **14** (1961) 27.
[25] HAUSER, J. J., CHEN, H. S., WASZCZAK, J. V., *Phys. Rev. B* **33** (1986) 3577.
[26] BUHLER, E., LAMPARTER, P., STEEB, S., *Z. Naturforsch.* **42a** (1987) 507.
[27] ANDONOV, P., CHIEUX, P., *J. Non Cryst. Solids* **93** (1987) 331.
[28] SACHDEV, S., NELSON, D. R., *Phys. Rev. B.* **32** (1985) 4592.
[29] REITER, H., RUPPERSBERG, H., SPEICHER, W., *Inst. Phys. Conf. Ser.* **30** (1977) 133.
[30] WASEDA, Y., *Inst. Phys. Conf. Ser.* **30** (1977) 230.
[31] WAGNER, C. N. J., RUPPERSBERG, H., *At. Energy Rev.* **1** (1981) 101.
[32] HAFNER, J., *J. Phys. F. : Met. Phys.* **18** (1988) 153.